



Simulation of brine discharge near sea farms in the Korea Strait

Youn-Jong Sun^a, Yang-Ki Cho^{b,*}, Kwang-Seok Park^c, Seok-Min Yoon^d, Jeong-Ki Moon^d

^a*School of Physical Environmental Mathematical Sciences, UNSW@ADFA, Canberra, ACT 2600, Australia*

^b*School of Earth and Environmental Sciences, Seoul National University, Seoul 151-742, Korea*

Tel. +82-2-880-6749; Fax: +82-2-871-3269; email: choyk@snu.ac.kr

^c*Department of Hybrid Materials Processing Research, Research Institute of Industrial Science & Technology, Pohang, Korea*

^d*Department of Environment Research, Research Institute of Industrial Science & Technology, Pohang 790-600, Korea*

Received 25 December 2011; Accepted 10 February 2012

ABSTRACT

Seawater desalination is a solution to water shortage problems for expanding coastal cities. However, seawater desalination leads to the discharge of brine into the coastal area. Brine of 60 psu in salinity might have an impact on the coastal ecosystem and environment. Accordingly, careful attention must be paid to determine the location of the outfall, especially as there are sea farms widely distributed along the Korean coast. In this study, the horizontal spreading of brine from different outfall positions was simulated using a three-dimensional circulation model to predict exactly the area affected by the brine. Model results showed that the brine spread offshore along the bottom layer as a result of its dense properties. It was found that the minimum distance of the outfall from the coast should be 0.5 km to avoid impact of salinity increase on sea farms and the coast within 0.5 psu. An alternative is dilution of the discharge by mixing with freshwater. If the salinity of the discharge is less than 40 psu, there would be little change in salinity for neighboring sea farms in this study.

Keywords: Seawater desalination; Brine discharge; Outfall position; Three-dimensional circulation model; Mixing

1. Introduction

Along with the current sharp economic growth in Korea, new land is required for living and industry in macro cities. The supply of river and underground water might be insufficient for the increasing population. Thus, seawater desalination is a possible solution to water shortage for an expanding coastal city. A desalination plant with a production capacity of

45,460 tons per day is scheduled to be built to supply water to a new city neighboring Busan, which is the second largest metropolis in Korea (Fig. 1).

However, seawater desalination leads to the discharge of high-concentration brine into the coastal area, which may have a negative impact on ecosystems and the environment. Accordingly, great care is necessary in determining the position of the outfall because there are sea farms widely distributed along the Korean coast. Purnama and Al-Barwani [1] simulated the behavior of brine to find suitable outfall positions which minimize the impact on beaches.

*Corresponding author.

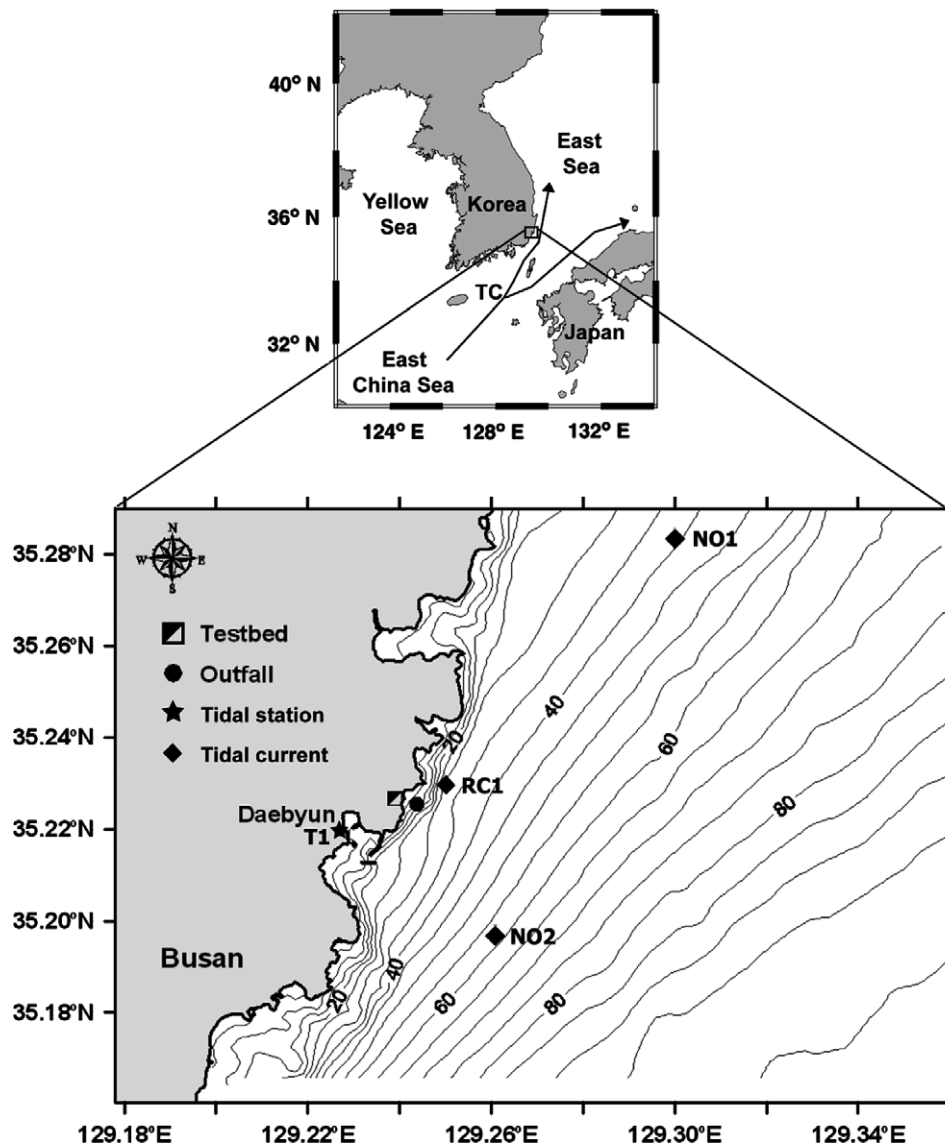


Fig. 1. Bottom topography of studied area. Contours with numbers show bottom topography. Modeled and observed surface elevation at T1 and currents at RC1, NO1, and NO2 were compared.

They demonstrated the horizontal distribution of salinity using a two-dimensional advection–diffusion equation. Mohamed [2] investigated the impact of brine disposal from desalination plants using a two-dimensional hydrodynamic model.

However, the two-dimensional model results could not resolve the vertical structure of brine spreading. If the outfall area is deep enough to maintain the stratification of the water column, the brine might produce different spreading patterns in each layer because of differences in density. The saline brine should mainly follow the bottom layer because of its density [3]. The depth of the studied area increases rapidly offshore and reaches 500 m. The depth of the potential outfall

position is shallower than 20 m (see the lower panel of Fig. 1).

In this study, the horizontal spreading of brine from different outfall positions was simulated to understand precisely the spreading limit of brine using a three-dimensional circulation model. The results from the model could be used to determine the most desirable outfall position to minimize the impact of brine waste on the coast and on sea farms [4].

2. Study area

The Korea Strait, which is the neighboring sea of the study area, connects the East China Sea with the

East Sea (Sea of Japan) (see the upper panel of Fig. 1). The Tsushima Current (TC), which originates from the Kuroshio, passes through the Korea Strait all year round. The TC splits into two branches after passing the Korea Strait [5]. One is the Nearshore Branch, flowing along the Japanese coast, and the other is the East Korean Warm Current, flowing along the Korean coast.

Tidal currents with a maximum speed of 50 cm s^{-1} is embedded in total currents of about 100 cm s^{-1} have been reported in the central region of the Korea Strait [6–8]. The current decreases greatly near the coast. The direction of the tidal current is southward during flood tide and northward during ebb tide.

3. Experimental design of the model

A Finite Volume Coastal Ocean Model (FVCOM) with an unstructured triangular grid (Fig. 2) was used for this study [9]. The model is composed of conservation of momentum, continuity, temperature, salinity, and density equations, similar to the primitive equations in other ocean models, which could be described to the following equations,

$$\begin{aligned} \frac{\partial u}{\partial t} + u \frac{\partial u}{\partial x} + v \frac{\partial u}{\partial y} + w \frac{\partial u}{\partial z} - fv \\ = -\frac{1}{\rho_0} \frac{\partial P}{\partial x} - \frac{\partial}{\partial z} \left(K_m \frac{\partial u}{\partial z} \right) + F_u \end{aligned} \quad (1.1)$$

$$\begin{aligned} \frac{\partial v}{\partial t} + u \frac{\partial v}{\partial x} + v \frac{\partial v}{\partial y} + w \frac{\partial v}{\partial z} + fu \\ = -\frac{1}{\rho_0} \frac{\partial P}{\partial y} + \frac{\partial}{\partial z} \left(K_m \frac{\partial v}{\partial z} \right) + F_v \end{aligned} \quad (1.2)$$

$$\frac{\partial P}{\partial z} = -\rho g \quad (1.3)$$

$$\frac{\partial u}{\partial x} + \frac{\partial v}{\partial y} + \frac{\partial w}{\partial z} = 0 \quad (1.4)$$

$$\frac{\partial T}{\partial t} + u \frac{\partial T}{\partial x} + v \frac{\partial T}{\partial y} + w \frac{\partial T}{\partial z} = \frac{\partial}{\partial z} \left(K_h \frac{\partial T}{\partial z} \right) + F_T \quad (1.5)$$

$$\frac{\partial S}{\partial t} + u \frac{\partial S}{\partial x} + v \frac{\partial S}{\partial y} + w \frac{\partial S}{\partial z} = \frac{\partial}{\partial z} \left(K_h \frac{\partial S}{\partial z} \right) + F_S \quad (1.6)$$

$$\rho = \rho(T, S) \quad (1.7)$$

where x , y , and z are east-west, north-south, and up-down directions at Cartesian coordinate, respectively; u , v , and w are the velocity component at x , y , and z , respectively. T , S , ρ , P , f , g denote the water temperature, salinity, density, pressure, coriolis coefficient, and gravity acceleration. K_m , K_h , F_u , F_v , F_T , and F_S mean the vertical eddy viscosity coefficient, thermal vertical eddy diffusion coefficient, horizontal momentums, thermal, and salt diffusion terms, respectively.

The Smagorinsky formula [10] and Mellor and Yamada level 2.5 turbulence closure schemes are used for horizontal viscosity and diffusivity, and vertical mixing. The Smagorinsky formula depends on grid size and the velocity gradient as follows

$$A_m = 0.5CA \sqrt{\left(\frac{\partial u}{\partial x}\right)^2 + \left(\frac{\partial v}{\partial x} + \frac{\partial u}{\partial y}\right)^2 + \left(\frac{\partial v}{\partial y}\right)^2} \quad (1.8)$$

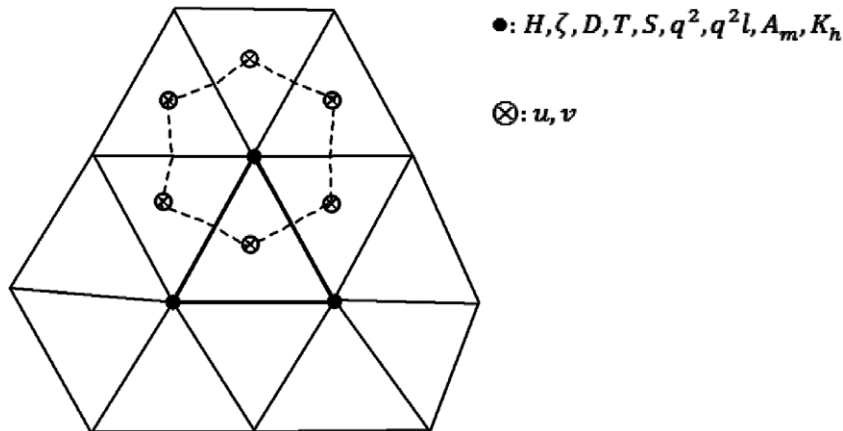


Fig. 2. Illustration on the unstructured triangular grid.

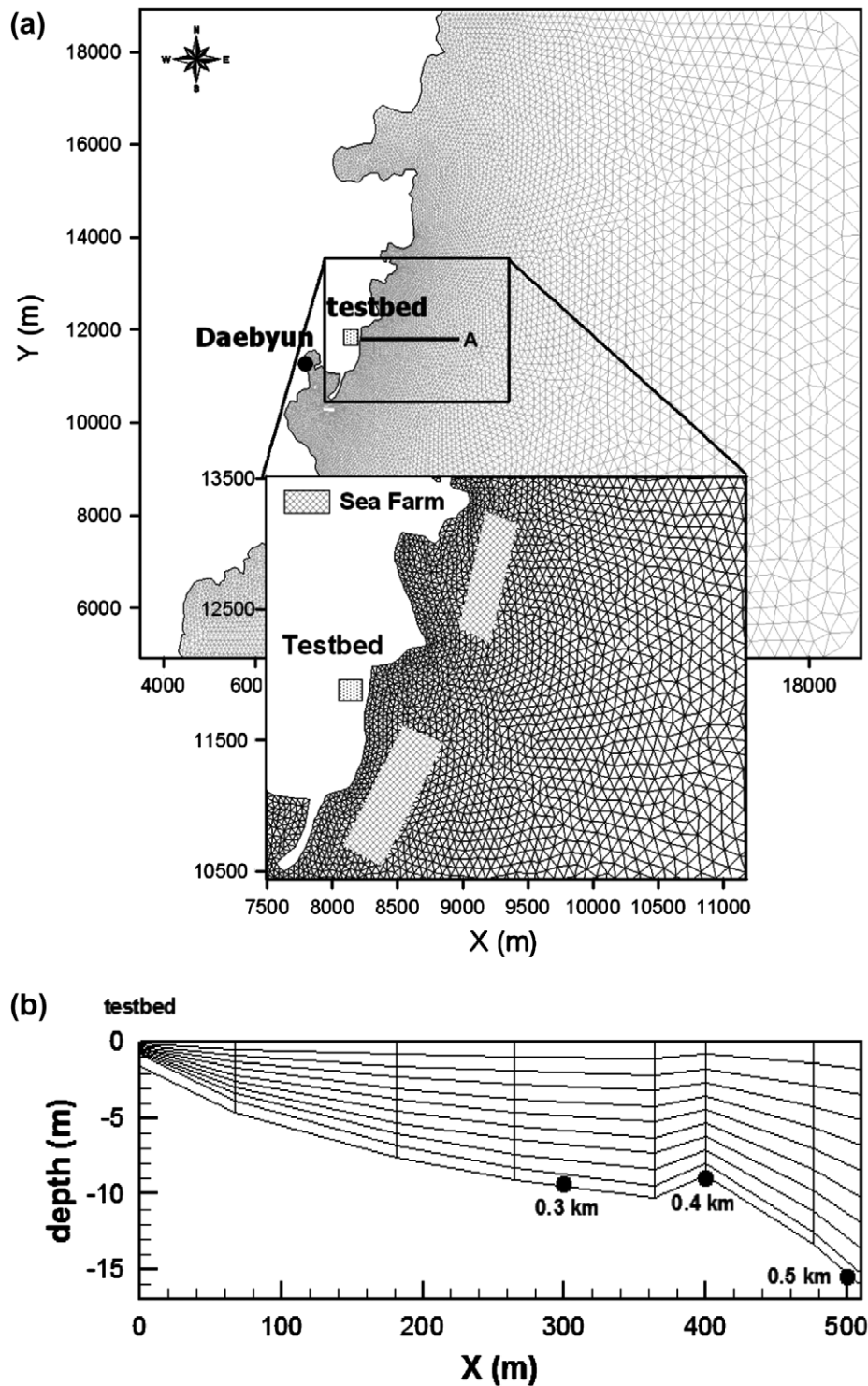


Fig. 3. Model domain of the study: (a) unstructured triangular grid cells and (b) vertical domain along the bold line A of the upper panel represented by a σ -coordinate system, except for the 10th layer. Circles are candidate sites for the most suitable outfall.

where, A_m is the horizontal eddy and thermal diffusion coefficient and C is constant. A is the area of the triangular grid. For vertical eddy viscosity and

vertical thermal diffusion coefficient, this model adopts Mellor and Yamada level 2.5 turbulent closure scheme [11] as follows

$$\frac{\partial q^2}{\partial t} + u \frac{\partial q^2}{\partial x} + v \frac{\partial q^2}{\partial y} + w \frac{\partial q^2}{\partial z} = 2(P_s + P_b - \epsilon) + \frac{\partial}{\partial z} \left(K_q \frac{\partial q^2}{\partial z} \right) + F_q \quad (1.9)$$

$$\frac{\partial q^2 l}{\partial t} + u \frac{\partial q^2 l}{\partial x} + v \frac{\partial q^2 l}{\partial y} + w \frac{\partial q^2 l}{\partial z} = l E_1 \left(P_s + p_b - \frac{\tilde{W}}{E_1} \epsilon \right) + \frac{\partial}{\partial z} \left(K_q \frac{\partial q^2 l}{\partial z} \right) + F_v \quad (1.10)$$

where $q^2 = (u^2 + v^2)/2$ is the turbulence kinetic energy and l is the turbulent macroscale.

K_{qv} , F_{qv} and F_l represent the vertical eddy diffusion coefficient of the turbulent kinetic energy, horizontal diffusion of the turbulent kinetic energy and macroscale, respectively. $P_s = K_m(u_z^2 + v_z^2)$ and $P_b = (gK_h \rho_z)/\rho_0$ are the shear and buoyancy produc-

tion terms of turbulent kinetic energy. $\epsilon = q^3/B_l l$ means the turbulent kinetic energy dissipation rate and $W = 1 + E_2 l^2 / (\kappa L)^2$ represents the wall proximity function [$L^{-1} = (\zeta - z)^{-1} + (H + z)^{-1}$, $\kappa = 0.4$: Von Karman constant, H : depth, ζ : free surface elevation (relative to $z=0$), D : total water depth ($= H + \zeta$)].

FVCOM with an unstructured triangular grid is useful for complex coastlines and sharp topographies like the south and west coasts of the Korean Peninsula [12–13]. A σ -coordinate system was used for the vertical layer and an unstructured triangular grid for the horizontal grid. The unstructured triangular grid is composed of three nodes, one element, and three sides (Fig. 4). The governing equation is basically solved by calculating the flux into the volume of a triangle. A finite volume method integrates advantages such as geometric flexibility of finite element method, and a simple discrete system and effective computation of finite difference method. Accordingly,

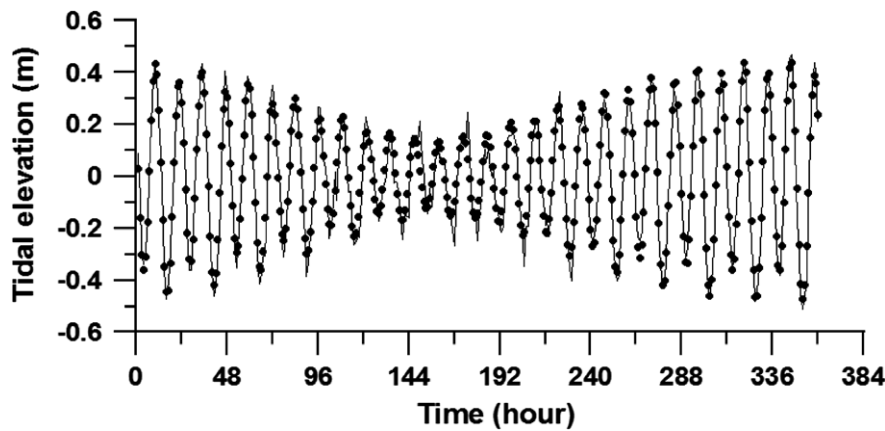


Fig. 4. Comparison of tidal elevation from observation (dotted mark) and modeled results (solid line) at station T1 (see the lower panel of Fig. 1).

Table 1

Comparison of observed and modeled tides. Error means a difference between observed and modeled values. ARE indicates an absolute relative error (%)

St.		M ₂				S ₂			
		Amp (cm)	Phase (°)	Error		Amp (cm)	Phase (°)	Error	
				ARE (%)				ARE (%)	
		Amp (cm)	Phase (°)			Amp (cm)	Phase (°)		
TO1 Daebyun port	Model	29.5	230.6			14.3	253.5		
	Obs.	29.1	226.2	0.4	4.4	14.1	256.6	0.2	-3.1
				1.4	1.9			1.4	1.2
TO1		K ₁				O ₁			
	Model	3.6	82.1			2.3	354.1		
	Obs.	3.1	86.2	0.5	-4.1	2.2	359.8	0.1	-5.7
				4.7	16.1			4.5	1.6

it functions well in describing mass, momentum, and conservation of heat and salt for a complex coastal area, and we can find the advantage through equations at the surface and bottom boundary as follows:

$$\frac{\partial T}{\partial z} = \frac{1}{\rho c_p K_h} [Q_n(x, y, t) - SW(x, y, \zeta, t)], \quad (1.11)$$

at $z = \zeta(x, y, t)$

$$\frac{\partial T}{\partial z} = \frac{A_H \tan \alpha}{K_h} \frac{\partial T}{\partial n}, \quad \text{at } z = -H(x, y) \quad (1.12)$$

where $Q_n(x, y, t)$ is a net flux of sea surface and $SW(x, y, 0, t)$ is a short radiation at the sea surface. c_p , A_H , α , and n are the specific heat of sea water, horizontal thermal diffusion coefficient, slope at bottom depth and perpendicular coordinate in the boundary, respectively.

$$\frac{\partial S}{\partial z} = -\frac{S(\hat{P} - \hat{B})}{K_h \rho} \cos \gamma, \quad \text{at } z = \zeta(x, y, t) \quad (1.13)$$

$$\frac{\partial S}{\partial z} = \frac{A_H \tan \alpha}{K_h} \frac{\partial S}{\partial n}, \quad \text{at } z = -H(x, y) \quad (1.14)$$

where \hat{P} and \hat{B} represent the precipitation and evaporation rates, and γ is $1/\sqrt{1 + |\nabla \zeta|^2}$.

The solid boundary condition for heat and salinity flux is as follows

$$v_n = 0; \quad \frac{\partial T}{\partial n} = 0; \quad \frac{\partial S}{\partial n} = 0 \quad (1.15)$$

where v_n is the velocity component normal in the boundary. The most general infinite difference method is featured by the temperature and salinity calculation in the bottom boundary for $\partial T/\partial z = \partial S/\partial z = 0$. However, it is hard for this equation to compute accurately in the irregular topography. Accordingly, infinite volume method is useful for computing the bottom slope and gradient of the temperature, and also salinity of Eqs. (1.12) and (1.14) in the irregular and complicate bottom topography using a green theorem.

Topographical data were obtained from the Korean Hydrographic and Oceanographic Administration (KHOA). There was a sharp bathymetric gradient 500 m away from the test bed for seawater desalination (see the lower panel of Fig. 1). The gradient was inclined towards the southeast (Fig. 1). The model domain was 14.7 and 14.0 km in the zonal and meridional directions, respectively, in the center of

Daebyun port (Fig. 3a). Grid cell sizes ranged from 6 to 1,043 m (Fig. 3a). Nine uniform sigma layers and a bottom fixed layer (10th layer, 0.8 m) were used to setup the vertical coordinate (Fig. 3b). Constant discharge ($0.547 \text{ m}^3 \text{ s}^{-1}$) for three proposed outfall sites (0.3, 0.4, and 0.5 km) was imposed. The corresponding depth of each location was 9.8, 8.4, and 15.5 m, respectively. Brine of 60 psu in salinity was released in the lowest layer and mostly followed this layer as a result of density. In reality, brine would be discharged as a 0.3 m^2 area source (through a 16-pipe diffuser system), but the outfall size for the model was set at 7.8 m^2 because of the model resolution. The relatively coarse grid of the large-scale model does not resolve the small-scale convective mixing processes in the near field. However, our interest was to understand the spreading range of the brine in the far field. For example, Signell et al. [14] successfully predicted the

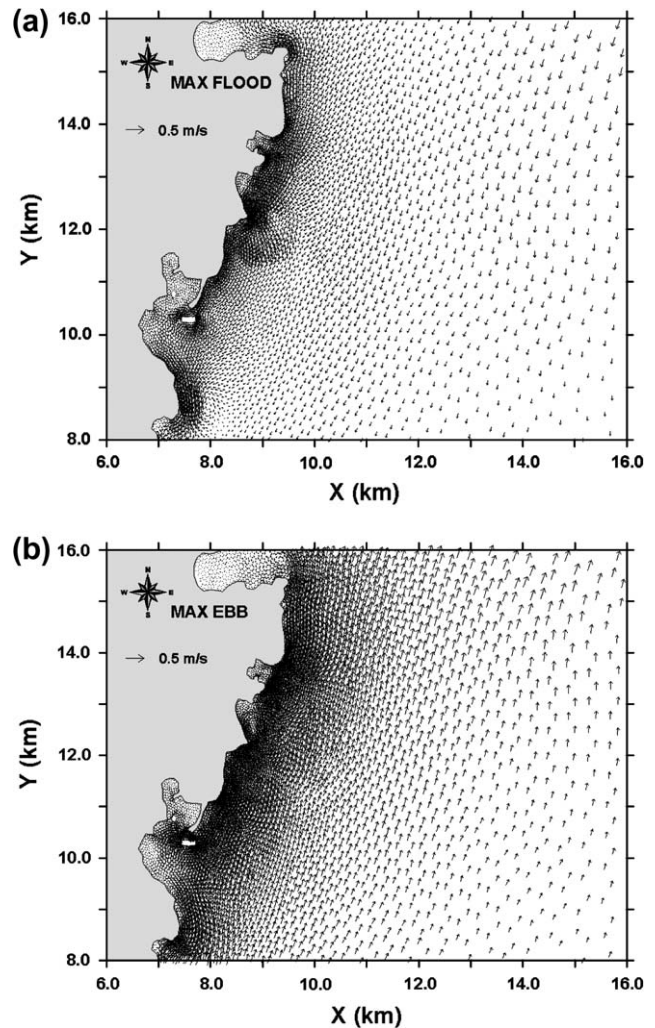


Fig. 5. Modeled current distribution around the studied area during (a) flood tide and (b) ebb tide.

salinity change resulting from the discharge of sewage effluent in Boston Harbor, using a three-dimensional hydrodynamic model.

For the initial computation, a cold start that tidal elevation was set at zero was given to all domains. The initial velocity field obtained from the history data was used for the initial conditions. The background temperature and salinity were set to 15°C and 34 psu, respectively, based on observational results for the winter in this region [15].

Four major tidal forcings (M_2 , S_2 , K_1 , and O_1) from NAO.99b were applied along the boundary to consider the tidal effect in the simulation. The calculated tide at Daebyun port was compared with observations. Time intervals would be set at 0.1 and 1.0 s for external and internal modes, respectively, satisfying CFL conditions.

4. Model verification

In order to verify model results with observed data, one point of tidal elevation (T1) and two points

(NO1 and NO2 in Fig. 1) of tidal current obtained from KHOA, and one point of tidal current (RC1 in Fig. 1) observed by National Fisheries Research Development Institute (NFRDI) were used. Fig. 4 shows the comparison of observation and model results on the tidal elevation at station T1 (see the lower panel of Fig. 1). The observation elevation was predicted using historic harmonic constituents (M_2 , S_2 , K_1 , and O_1) analyzed during one month (1 April 1984–30 April 1984) at T1. Table 1 shows the comparison of modeled and observed tides. Error means a difference between modeled and observed values. ARE indicates an absolute relative error (%). There was little difference in the amplitudes and phases, less than 0.5 cm and $\pm 6^\circ$, respectively.

KHOA observed the current around Busan (see Fig. 1) for 16 days in 2004 and reported it flowing northeast during ebb tide and southwest during flood tide [16]. This implies that the TC flowing northeast leads to stronger flow during ebb tide than during flood tide.

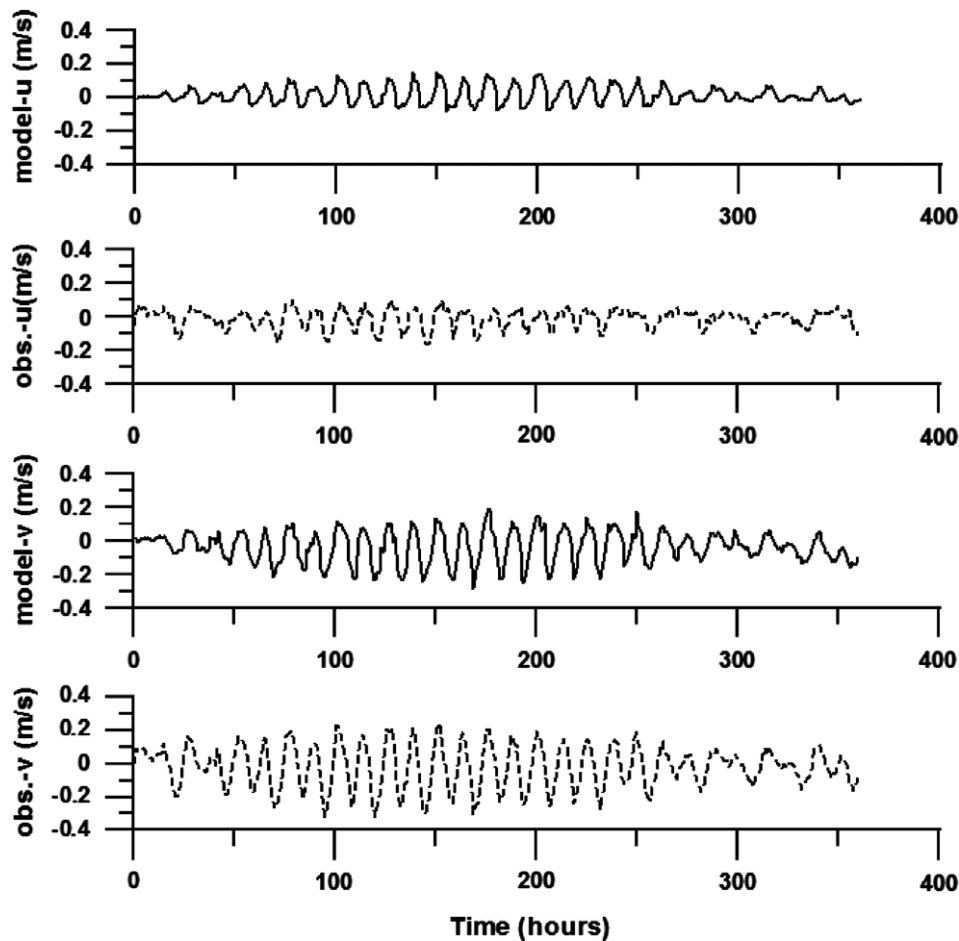


Fig. 6. Comparison of velocity from observation (second and fourth panels with dotted line) and modeled results (first and third panels with solid line) at station RC1.

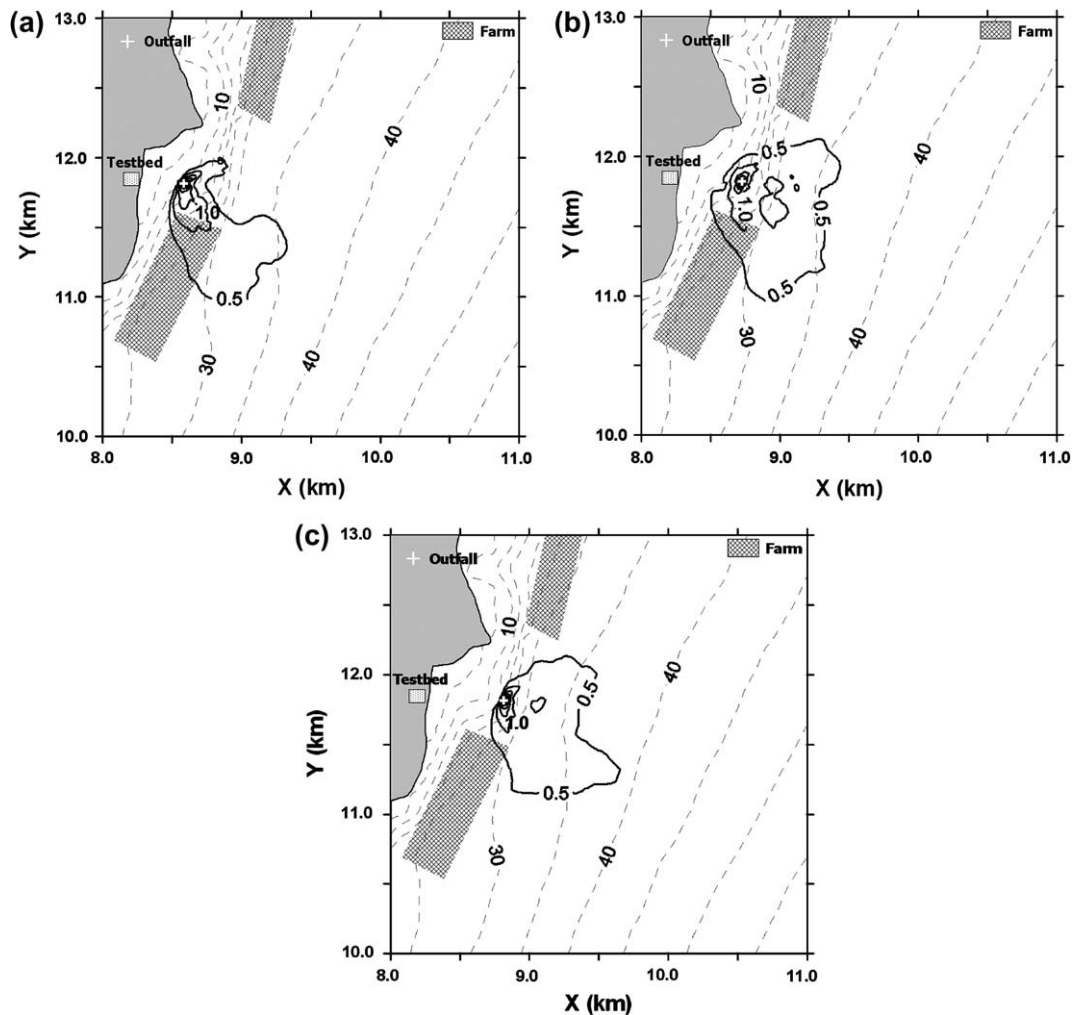


Fig. 7. Horizontal distribution of saline water discharged from the different outfall locations according to the distance of the outfall from the coast: (a) 0.3 km, (b) 0.4 km, and (c) 0.5 km. Broken lines are bathymetric contours at 5 m intervals. Solid contours represent increased salinity in the bottom layer.

The flow in the study area, which is greatly controlled by ocean currents, has large variations. The observed maximum current speeds during the spring tide period computed by harmonic analysis were 38.9 and 52.4 cm s^{-1} at NO1 and NO2, respectively. The observed mean currents during 2 months (1 April 2004–31 May 2004, using RCM9) were 34.9° , 27.0 cm s^{-1} and 23.0° , 29.2 cm s^{-1} at NO1 and NO2, respectively [16]. This result shows that the modeled current was well reproduced (Fig. 5).

In addition, model results were compared with the velocity obtained from RCM9 deployed at 25 m depth of station RC1 (Fig. 1) during 15 days (10 February 2010–25 February 2010) by NFRDI (Fig. 6). We found that the amplitude variations of U - and V -velocities were reproduced well by the model. In addition, we calculated the residual current based on modeled and

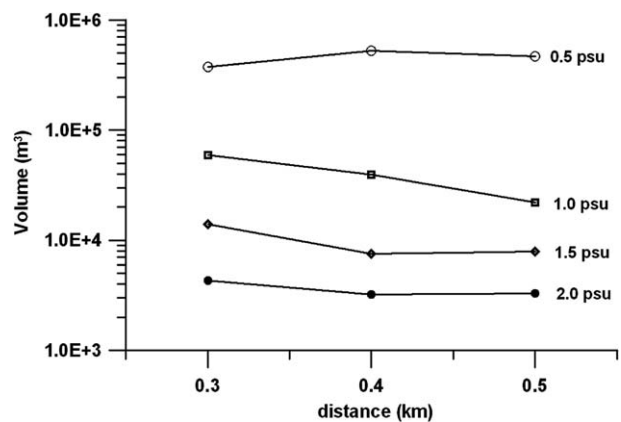


Fig. 8. Variation in volume of saline water, according to the distance of the outfall from the coast. The reference value (psu) to the right of each line is the increased salinity above the background salinity of 34 psu.

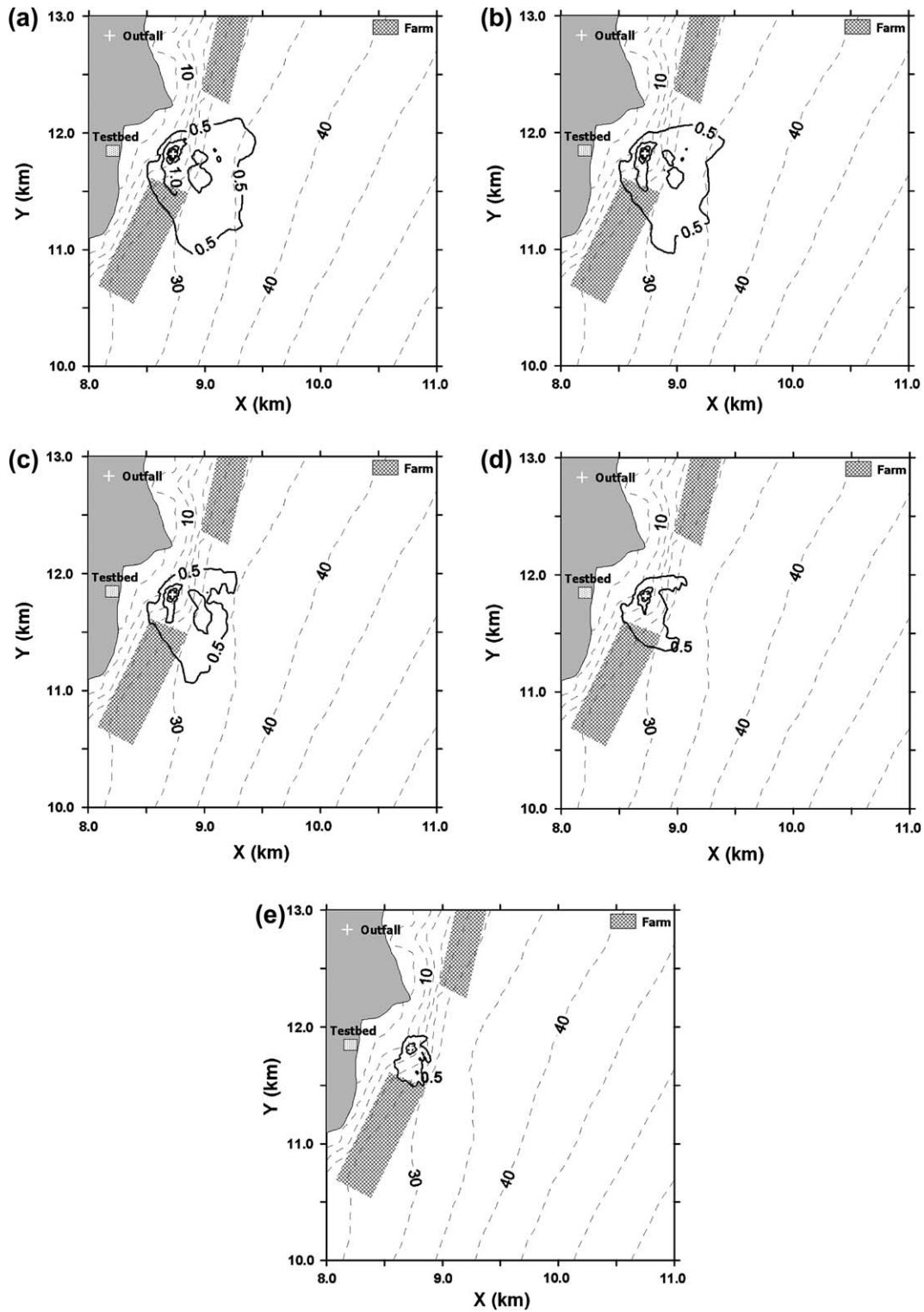


Fig. 9. Horizontal distribution of saline water discharged from the outfall according to the different salinities and volumes of the discharge: (a) 60 psu, $0.55 \text{ m}^3 \text{ s}^{-1}$, (b) 55 psu, $0.60 \text{ m}^3 \text{ s}^{-1}$, (c) 50 psu, $0.65 \text{ m}^3 \text{ s}^{-1}$, (d) 45 psu, $0.73 \text{ m}^3 \text{ s}^{-1}$, and (e) 40 psu, $0.82 \text{ m}^3 \text{ s}^{-1}$. Broken lines are bathymetric contours at 5 m intervals. Solid contours represent increased salinity at the bottom layer.

observed velocities (Fig. 6) because the residual current affects chiefly the transport of saline water. The values showed -0.7 (1.4) cm s^{-1} and -1.7 (-3.2) cm s^{-1} toward the east-west and north-south directions, respectively, from observed (modeled) results.

5. Distribution of brine corresponding to a different outfall location

The spreading pattern of brine, according to the location of the outfall was compared. Fig. 7 shows the horizontal distribution of the maximum difference of salinity between the background water and the saline water that flowed out from the outfall during the model run (16 days). The maximum difference was computed at each cell of the whole model domain. The imposed temperature and salinity along the open boundary were 15°C and 34 psu, respectively, without spatial variations.

The spreading of the plume of effluents from the outfall 0.3 km away from the coast was directed mainly to the southeast and partly to the northeast, like a thin branch of a tree (Fig. 7a). The saline water from the outfall 0.4 km away from the coast spread mainly to the southeast and the northeast, like a mushroom-shaped plume (Fig. 7b). The plume of the saline water from the outfall 0.5 km off the coast was towards the southeast and the northeast (Fig. 7c). The main direction of the spreading was along the deep area because of the density of the brine [3]. The residual current also might have had an influence on the transport and dispersion of saline water from the outfall [2].

Fig. 8 shows the variations in volume for saline water depending on the outfall location's distance from the coast. The reference value for salinity was the increased salinity above the background salinity of 34 psu. The volume of saline water was the sum of the areas with a higher salinity than the reference value in all cells for 16 days. The defined volumes for saline water mostly decreased with the distance of the outfall from the coast, whereas the volume defined by 0.5 psu increased with distance. This phenomenon resulted from active mixing by relatively strong currents offshore, as shown in Fig. 3. The strong mixing decreases the core volume (salinity greater than 1.0 psu) but increases the diluted volume (salinity less than 0.5 psu).

6. Effect of diluted discharge on salinity change

Dilution of the brine with freshwater from sewage treatment plants is known to be one of the best available technologies to reduce the impact of the

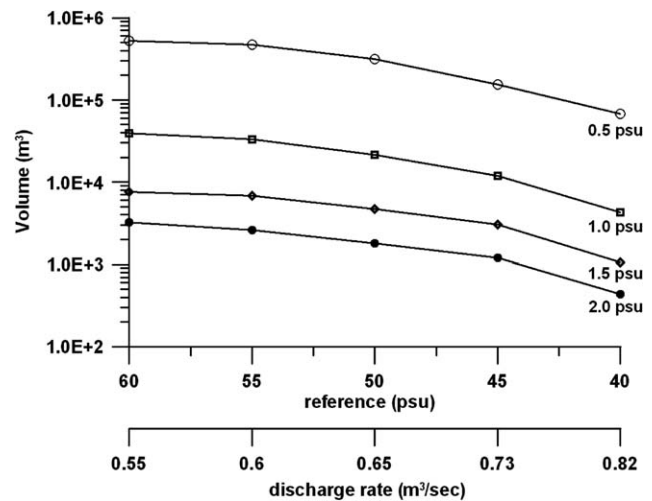


Fig. 10. Variation in volume of saline water, depending on different discharge rates and salinities. The reference value is the increased salinity above the background salinity of 34 psu.

discharge on the neighboring sea. We assume that the salinity of the discharge decreases from 60 to 40 psu and the volume of discharge increases because of mixing with freshwater.

Fig. 9 shows the horizontal distribution of the increased salinity at the bottom layer under different salinities and volumes of discharge. The discharge rate is increased as the salinity of the discharge decreases to keep the total salt from the outfall constant. The saline area decreases rapidly as the mixing ratio increases. The isohaline of 0.5 psu does not reach the sea farm when the salinity of the discharge is 40 psu.

The variations in the volume of saline water based on different discharge rates and salinities from the outfall were plotted (Fig. 10). The figure shows that the volume defined for all salinities decreases. Active mixing by increasing the discharge rate might reduce the area of salinity neighboring the sea farm. These simulation results suggest that mixing the brine with freshwater is an alternative solution for mitigating the environmental impact in the region.

7. Conclusions

A three-dimensional circulation model is a useful tool for understanding the behavior of brine from an outfall and for determining the location that best minimizes its impact upon the local area. This model simulated the behavior of brine spreading offshore and found that it follows deep areas because of its density. To avoid the negative impact of brine discharge on

the coast and on sea farms, an outfall at a distance of more than 0.5 km from the coast was found to be desirable. Another practical discharging option was dilution of the brine water with treated water of low salinity from a sewage treatment plant. In this study, if the salinity of the discharge was less than 40 psu, there would be almost negligible change in salinity for neighboring sea farms, even though the total salt discharge would still be the same.

Further work testing the sensitivity of the model will provide more concrete model predictions. Although this simulation enabled us to determine the positions for outfalls, a more realistic simulation including vertical stratification and finer resolution remains as a challenge.

Acknowledgments

This work was supported by Seawater Engineering & Architecture of High Efficiency Reverse Osmosis (seaHERO). Y.-K. Cho was partly supported by the project titled “Long-term change of structure and function in marine ecosystems of Korea” funded by the Ministry of Land, Transport and Maritime Affairs, Korea.

References

- [1] A. Purnama, H.H. Al-Barwani, Spreading of brine waste discharge into the Gulf of Oman, *Desalination* 195 (2006) 26–31.
- [2] K.A. Mohamed, Model investigation on the impact of Raha Beach development on Umm Al Nar Power and Desalination Plant, *Desalination* 212 (2007) 357–366.
- [3] Water Corporation, Southern seawater desalination project, Chapter 8, Marine factors, Environmental impact assessment public environmental review (2008) 180–187. Available from: www.watercorporation.com.au/D/desal2_per.cfm.
- [4] R. Danoun, *Desalination Plants: Potential impacts of brine discharge on marine life*, University of Sydney, 2007, p. 55.
- [5] Y.K. Cho, K. Kim, Branching of the Tsushima Current in the Korea Strait, *J. Phys. Oceanogr.* 30 (2000) 2788–2797.
- [6] A. Isobe, S. Tawara, A. Kaneko, M. Kawano, Seasonal variability in the Tsushima Warm Current, *Tsushima-Korea Strait*, *Cont. Shelf Res.* 14 (1994) 23–35.
- [7] W.J. Teague, H.T. Perkins, G.A. Jacobs, J.W. Book, Tide observations in the Korea-Tsushima Strait, *Cont. Shelf Res.* 21 (2001) 545–561.
- [8] W.J. Teague, G.A. Jacobs, H.T. Perkins, J.W. Book, K.I. Chang, M.S. Suk, Low frequency current observations in the Korea Strait, *J. Phys. Oceanogr.* 32 (2002) 1621–1641.
- [9] C. Chen, H. Liu, R.C. Beardsley, An unstructured, finite-volume, three-dimensional, primitive equation ocean model: Application to coastal ocean and estuaries, *J. Atmos. Ocean Technol.* 20 (2003) 159–186.
- [10] J. Smagorinsky, General circulation experiments with the primitive equations, I: The basic experiment, *Mon. Weather Rev.* 91 (1963) 99–164.
- [11] G.L. Mellor, T. Yamada, Development of a turbulence closure model for geophysical fluid problems, *Rev. Geophys. Space Phys.* 20 (1982) 851–875.
- [12] Y.J. Sun, A. Isobe, Lagrangian H/U³ values computed around tidal fronts using a fine-resolution numerical model and ferryboat-monitored SST dataset, *J. Phys. Oceanogr.* 38 (2008) 2575–2586.
- [13] T.W. Kim, Y.K. Cho, Calculation of heat flux in a macrotidal flat using FVCOM, *J. Geophys. Res.* 116 (2011) C03010.
- [14] R.P. Signell, H.L. Jenter, A.F. Blumberg, Predicting the physical effects of relocating Boston’s sewage outfall, *Estuar. Coast. Shelf Sci.* 50 (2000) 59–72.
- [15] Y.K. Cho, K. Kim, Structure of the Korea Strait Bottom Cold Water and its seasonal variation in 1991, *Cont. Shelf Res.* 18 (1998) 791–804.
- [16] Korea Hydrographic and Oceanographic Administration, Technical reports of oceanographic research, 2004, 568.